On the heat capacity of adsorbed phases using molecular simulation

G. R. Birkett and D. D. Do

Citation: The Journal of Chemical Physics **126**, 064702 (2007); doi: 10.1063/1.2434149
View online: http://dx.doi.org/10.1063/1.2434149
View Table of Contents: http://scitation.aip.org/content/aip/journal/jcp/126/6?ver=pdfcov
Published by the AIP Publishing

On the heat capacity of adsorbed phases using molecular simulation

G. R. Birkett and D. D. Do[a)]
Department of Chemical Engineering, University of Queensland, St. Lucia, Queensland 4072, Australia

(Received 26 October 2006; accepted 21 December 2006; published online 8 February 2007)

The heat capacities of argon, ammonia, and methanol on carbon black at 87.3, 240, and 300 K, respectively, have been investigated. The carbon black surface has been modeled with and without carbonyl groups. Part of this investigation is a decomposition of the heat capacity into its contributions from the different interaction potentials of an adsorption system. All systems show a spectrum of heat capacity versus loading, and this behavior depends on the carbonyl configuration present on the surface. For methanol and ammonia the variation of the heat capacity between the two for the same carbonyl configurations is greater than the variation in the heat of adsorption. Heat capacities of methanol and ammonia are generally dominated by fluid-fluid interactions due to the strong association of fluid particles through hydrogen bonding. The difference in the heat capacity behavior of the two fluids is an indicator of their different clustering behaviors on the carbon black surface. The presence of carbonyl groups reduces the fluid-fluid contributions to the heat capacity. This is due to the compensation of fluid-fluid interactions with fluid-functional group interactions. At 87.3 K a first layer transition to a solidlike state is present for argon and results in a large peak in the heat capacity on a bare surface. The presence of functional groups greatly reduces this peak in the heat capacity by disrupting the packing of argon on the surface and preventing a transition to a solidlike state. © *2007 American Institute of Physics*. [DOI: 10.1063/1.2434149]

I. INTRODUCTION

Equilibrium studies of adsorption are generally concerned with two quantities: the amount adsorbed versus pressure and the heat of adsorption. The importance of these two quantities is obvious for their direct practical importance to adsorption and catalyst processes and also for the validation of various potential models. For classical models, this is a validation of the model itself, whereas for simulation studies we seek to validate adsorbate and adsorbent potential models to be applied using Monte Carlo or molecular dynamics simulations.[1] Recently we calculated another thermodynamic property of adsorption using molecular simulation when studying the adsorption of methanol and ethanol on carbon black,[2] the heat capacity. This showed some very interesting behavior in the heat capacity and its variation with the functional groups present on the surface. This has prompted a further study to investigate the effect of the functional groups on the heat capacity of a further two fluids, argon and ammonia. The results of this are presented together with the results of the study on methanol to present some insight into the range of heat capacity behavior on carbon black and how it changes with the degree of fluid-fluid interaction on the surface (argon < ammonia < methanol).

II. POTENTIAL MODELS

A. Fluid potential models

Rigid polyatomic models are used for methanol and ammonia, and a single site Lennard Jones (LJ) model is used for argon. The methanol and ammonia models are characterized by the positions of their LJ and Coulomb sites and the parameters of these sites. The methanol model used in this study is the "TraPPE-UA" potential presented by Chen *et al.*[3] This is a model optimized for the phase coexistence of methanol based on common parameters with other alcohols. This model, when originally proposed, took into account the effect of bond angle bending, but this has been assumed to be negligible and not taken into account for this paper. The model used for ammonia is that of Kristof *et al.*[4] This model has been optimized to reproduce the vapor-liquid equilibrium data of ammonia above 281 K by its authors. The argon model used is that of Michels *et al.*[5] with a LJ collision diameter σ of 0.3405 nm and a reduced LJ well depth ε/k_B of 119.8 K (where k_B is Boltzmann's constant). The values of the molecular parameters for the methanol and ammonia models are given in Table I.

The vapor-liquid equilibrium properties of the three

TABLE I. Molecular parameters of methanol and amonia models.

Parameter	Site	Methanol	Site	Ammonia
σ (mm)	CH_3	0.375	N	0.3385
ε/k_B (K)	CH_3	98.0	N	170.0
σ (nm)	O	0.302	H	···
ε/k_B (K)	O	93.0	H	···
$q(e)$	CH_3	0.265	N	−1.035
$q(e)$	O	−0.700	H	0.345
$q(e)$	H	0.435	···	···
R (nm)	C–O	0.1430	N–H	0.101 24
R (nm)	O–H	0.0945	···	···
Angle (deg)	COH	108.5	HNH	106.68

[a)]Author to whom correspondence should be addressed. Tel.: +61-7-3365-4154. Fax: +61-7-3365-2789. Electronic mail: duong@cheque.uq.edu.au

TABLE II. Saturation properties of argon, ammonia, and methanol models from GEMC simulations (bracketed values are uncertainty of calculations).

Parameter	Argon	Ammonia	Methanol
T (K)	87.3	240	300
P^{VAP} (kPa)	94 (14)	107 (19)	16.5 (1.9)
ρ^V (kmol/m^3)	0.133 (0.02)	0.054 (0.01)	0.008 (0.001)
ρ_L (kmol/m^3)	34.95 (0.16)	40.47 (0.21)	24.1 (0.1)
ΔH^V (kJ/mol)	6.63 (0.03)	24.45 (0.13)	38.6 (1.0)
C_V^L (J/mol K)	21.1 (0.6)	41.0 (3.5)	47.7 (4.0)

models have been calculated using Gibbs Ensemble Monte Carlo (GEMC).[6,7] These properties are given in Table II. The vapor pressures for argon, ammonia, and methanol agree fairly well with the experimental values of 101, 102, and 18.7 kPa, respectively.

B. Surface model

The simulation cell is bound in the z direction by the walls of a slit pore. Only one of the walls of the pore has an attractive interaction with the fluid molecules. This pore wall interacts with a fluid molecule according to the Steele 10-4-3 potential[8] given by

$$u_1^{\text{surf}} = \sum_{a=1}^{A} 2\pi\rho_s\varepsilon_{is}^a(\sigma_{is}^a)^2\Delta\left[\frac{2}{5}\left(\frac{\sigma_{is}^a}{z_i^a}\right)^{10} - \left(\frac{\sigma_{is}^a}{z_i^a}\right)^4 - \left(\frac{\sigma_{is}^{a\,4}}{3\Delta(z_l^a + 0.61\Delta)^3}\right)\right], \quad (1)$$

where u_i^{surf} is the interaction between a molecule i and the carbon surface, A is the number of LJ sites on molecule i, ρ_s is the graphite's carbon density, Δ is the separation distance between graphite layers, z_i^a is the shortest distance between LJ site a and the surface, and ε_{is}^a and σ_{is}^a are the LJ well depth and collision diameter between site a and the surface calculated using the Lorentz-Berthelot mixing rule.[9] The molecular parameters for the carbon wall Steele potential are given in Table III.

The opposing wall has no attractive term and has only an effectively infinite repulsion for molecules that cross the pore wall. The simulation cell is repeated periodically in the x and y directions to approximate an infinite pore. The model pore has a width of 5.0 nm and a length in the simulation cell of 7.5 nm. A simulation cell length 1.5 times the pore width has been observed to be sufficient by Jorge and Seaton[10] to avoid observable finite size effects and this has been the experience of the authors as well. A pore width of 5.0 nm allows a good approximation of carbon black with the opposite hard wall having no observable effect on the adsorption at the Steele potential surface until many layers are formed at pressures very close to the vapor pressure of the fluid.

TABLE III. Molecular parameters of carbon surface used in the Steele 10-4-3 equation.

σ_{ss} (nm)	ε_{ss}/k_B (K)	ρ_s (nm^{-3})	Δ (mm)
0.34	28.0	114	0.335

TABLE IV. Molecular parameters of carbonyl group.

ε/k_b (K)	σ (nm)	q$^-$ (e)	q$^+$ (e)	R_{CO} (nm)
105.8	0.296	−0.5	0.5	0.1233

C. Carbonyl functional groups

The only type of functional group considered in this study is carbonyl. This is modeled with a single LJ site at the oxygen, a distance R_{CO} perpendicular to the carbon surface, a positive charge on the surface, and negative charge at the oxygen. The parameters for the carbonyl group are taken from the optimized potentials for liquid simulation potential model for amino acids[11] and are given in Table IV.

The configuration of functional groups has previously been observed to strongly affect the adsorption isotherms and isosteric heats of water,[12,13] ammonia,[14] and ethanol and methanol.[2] In the study of ethanol and methanol by Birkett and Do[2] it was also shown that the functional groups strongly affect the heat capacity of the adsorbed alcohols on carbon black. The different carbonyl configurations used in this study are presented in Fig. 1.

The LJ interaction parameters between fluid molecules and the carbonyls are calculated using the Lorentz-Berthelot mixing rule. Carbonyls, as opposed to other functional groups, were chosen for their simplicity and that carbonyls represent a large percentage of the functional groups on carbon blacks treated at high temperatures.[15,16] The simplicity of carbonyls offers a very small saving in computational cost compared with hydroxyl or carboxylic groups, but more importantly they reduce the parameters that are required. Carbonyls can only be adjusted by their positions, whereas hydroxyl and carboxyl groups must have their orientation specified. This combined with the fact that comparison is being made between simulation and experiments on carbon blacks heat treated at high temperatures makes carbonyl a good choice for this preliminary study. The surface concentration equivalents of using 5, 9, 45, and 49 carbonyls in the simulation are 0.15, 0.27, 1.33, and 1.45 μmol/m^2.

III. SIMULATION DETAILS

Monte Carlo simulations were conducted using the Grand Canonical Monte Carlo (GCMC) ensemble.[9] For some isotherm points, the aggregation-volume-bias (AVB) sampling proposed by Chen and Siepmann[17] was used. In this simulation study we used the scheme termed AVBMC2 by these authors. We will refer to a move performed under

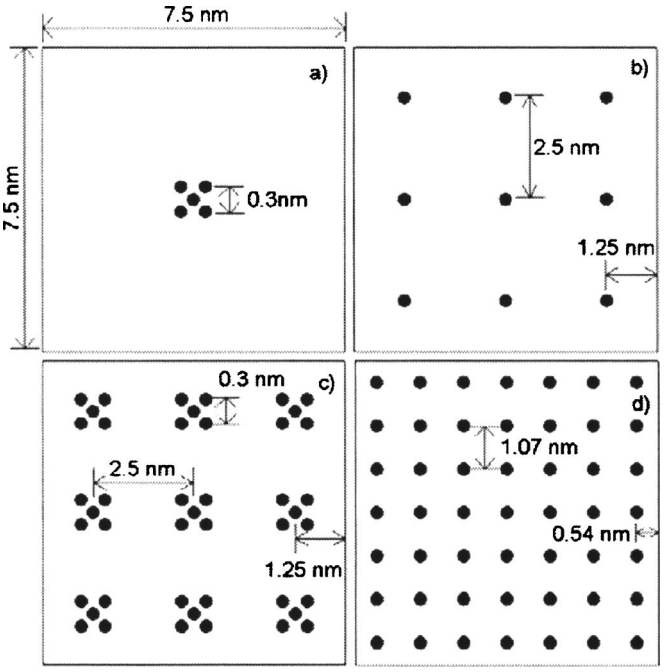

FIG. 1. Configurations of carbonyls (represented as filled circles) on the bottom plane of the pore: (a) group of 5 carbonyls located at the center of the pore wall, (b) 9 evenly spaced carbonyls, (c) nine evenly spaced groups of 5 carbonyls, and (d) 49 evenly spaced carbonyls. All configurations have the same box length of 7.5 nm.

the AVBMC2 scheme as an AVB move. The chemical potentials used in the simulations were the ideal chemical potentials of the pressures reported, a reasonable approximation for the low pressures studied. Simulations were conducted at 87.3 K with pressures from 0.001 to 30 kPa for argon (P^{VAP}=94 kPa), at 300 K with pressures from 0.001 to 5 kPa for methanol (P^{VAP}=16.7 kPa), and at 240 K with pressures from 0.01 to 52 kPa for ammonia (P^{VAP} =107 kPa). Each simulation isotherm point was equilibrated until the number of molecules and energy of the system reached a stable value. From this point ensemble data were collected over a minimum of $2.5\times10^{7}-6\times10^{9}$ Monte Carlo steps, depending on the point on the isotherm. Steps used were translations, rotations (for ammonia and methanol), insertions, deletions, or AVB moves. AVB moves were used only for ammonia and methanol where the sampling of clusters is important for the calculation of isosteric heats and heat capacities. When they were used, the number of attempted AVB moves was set to achieve one successful swap per 100 moves. If this could not be achieved, the maximum number of AVB moves was set to five times the number of translations and rotations. The number of insertions was set to give four successful insertions per 100 moves. If this could not be achieved, the maximum number of insertions was set to five times the number of translations and rotations. The number of deletions was set equal to the number of insertions. Once an isotherm point was completed, its final configuration was used as the initial configuration of the next isotherm point, mimicking the experimental adsorption procedure. Uncertainties of ensemble averages are estimated by calculating the variance of the ensemble quantities when they are broken into ten evenly sized blocks. Uncertainties presented as error bars in figures hereafter are the variances calculated by this technique.

No long range corrections were used for either dispersion (LJ) or electrostatic interactions. This is due solely to the greatly increased computation time required for isotherms using appropriate long range corrections for the Coulomb interactions such as the technique of Heyes and Van Swol[18] and Jorge and Seaton[19] or a two dimensional Ewald-type sum.[19,20] Shevade *et al.*[21] have reported a small difference in the potential of adsorption systems between using a long range correction and a two dimensional Ewald-type correction,[20] and ignoring the long range corrections. Citing an increase in computational cost of two orders of magnitude, long range corrections were not used by Shevade *et al.* Long range corrections have not been used for many other simulation studies of water in carbon pores.[22–26] LJ interactions were cut at a cylindrical cutoff in the *x*-*y* plane at a distance equal to half the simulation box length (3.75 nm for all simulations). Coulomb interactions were cut on a molecular basis using the separation of specific atom sites on the molecules (nitrogen for ammonia and oxygen for methanol). So if two molecules satisfied this cutoff criterion, all Coulomb interactions were counted between the particles even if some charge separations were greater than the cutoff in the *x*-*y* plane. Cutoffs on an atomistic charge-charge basis would lead to spuriously high interactions in the case where not all charges on a molecule are used in the interaction potential calculation. The same cutoffs were applied to the interactions of fluid molecules with carbonyl sites. The isosteric heat was calculated using[27]

$$q_{st} \cong \frac{\langle NU\rangle - \langle N\rangle\langle U\rangle}{\langle N^2\rangle - \langle N\rangle\langle N\rangle} + k_B T. \tag{2}$$

The first term in Eq. (2) can also be splitted into the different contributions to the system potential energy U. The three contributions to the potential energy are the fluid-fluid interactions, the fluid-surface interactions, and the fluid-functional group interactions. Replacing U in Eq. (2) with one of these contributions to the potential and discounting the second term will give its contribution to the isosteric heat. The heat capacity of the adsorbed alcohols was also calculated. The constant volume heat capacity C_V is calculated using[9]

$$C_V = \frac{(\langle U^2\rangle - \langle U\rangle\langle U\rangle) - [(\langle UN\rangle - \langle U\rangle\langle N\rangle)^2/\langle N^2\rangle - \langle N\rangle\langle N\rangle]}{\langle N\rangle k_B T^2} + 1.5k_B. \tag{3}$$

To investigate the origin of changes to the heat capacity, it is informative to calculate the contributions to the heat capacity from each component of the system interaction potential. The individual contributions to the heat capacity can be calculated using[28]

$$C_V^x = \frac{(\langle UU_x\rangle - \langle U\rangle\langle U_x\rangle) - [(\langle UN\rangle - \langle U\rangle\langle N\rangle)(\langle U_xN\rangle - \langle U_x\rangle\langle N\rangle)/\langle N^2\rangle - \langle N\rangle\langle N\rangle]}{\langle N\rangle k_B T^2}. \quad (4)$$

IV. RESULTS AND DISCUSSION

Simulated adsorption isotherms for argon at 87.3 K, ammonia at 240 K, and methanol at 300 K are presented in Figs. 2–4, respectively. Each of these figures shows the results for a bare graphite (Steele) surface and surfaces with the carbonyl configurations shown in Fig. 1.

The effect of functional groups on the adsorption isotherm of argon in Fig. 2 is small but certainly observable for the case of 49 evenly distributed carbonyls or nine groups of 5 carbonyls. This difference is seen in the region of submonolayer coverage. Once monolayer coverage is achieved the difference between all the isotherms is small. The difference between the isotherms for the surface with five carbonyls or nine evenly spread carbonyls and that of the bare surface is indistinguishable in the main plot of Fig. 2, but the inset shows that some small difference does exist at low pressure due to the additional LJ attraction of the carbonyl groups. In the Henry law region, the adsorption is increased by 6%, 9%, 55%, and 56% by 5 grouped carbonyls, 9 evenly distributed carbonyls, 49 evenly distributed carbonyls, and nine groups of 5 carbonyls, respectively. So the grouped carbonyls have a greater effect on the adsorption on a per carbonyl basis but not by much.

The effect of the carbonyls on the adsorption isotherms of ammonia[14] and methanol[2] has been previously presented but are presented in Figs. 3 and 4, respectively, for ease of discussion. Figures 3 and 4 show that the carbonyl groups have a very large effect on the adsorption isotherm of ammonia and methanol. Without functional groups, ammonia adsorption is quite low until 52 kPa, where the ammonia condenses to approximately monolayer coverage. The addition of carbonyl groups increases the amount adsorbed for all pressures. Closely grouped carbonyls cause the greatest increase in the amount adsorbed initially due to their higher interaction potential with individual molecules. The more evenly spaced groups eventually cause greater adsorption since the distance between initially formed clusters is reduced facilitating the agglomeration of theses clusters. The methanol and ammonia adsorption isotherms are clearly different with methanol having a continual increase in the amount adsorbed up to monolayer coverage for the bare surface. However, the effect of the carbonyl groups on methanol adsorption is similar to the effect on ammonia.

Now the heats of adsorption of the three fluids have also been calculated using Eq. (2). These are presented in Figs. 5–7 for argon, ammonia, and methanol, respectively. The heats of adsorption for ammonia[14] and methanol[2] have been previously presented and are presented again here for discussion.

For argon in Fig. 5, we see a typical behavior of isosteric heat versus loading for noble gases on graphite.[29] The heat of adsorption initially increases with adsorption due to increasing fluid-fluid interaction in the monolayer. When monolayer coverage is approached, the heat of adsorption decreases due to the reduction of fluid-solid interaction of molecules subsequently adsorbed which increasingly occurs in the second layer. A local minimum is seen shortly after monolayer coverage after which the heat of adsorption increases again due to increased fluid-fluid interaction in the second layer. Now the heat of adsorption is quite similar for all carbonyl configurations. However, there are some observable differences.

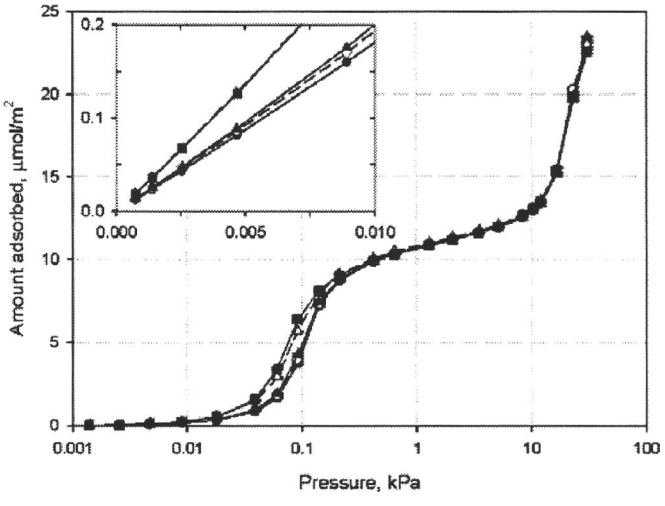

FIG. 2. Adsorption isotherms from simulation for argon at 87.3 K on graphite (modeled using Steele potential) with no functional groups (filled circles and solid line), five grouped carbonyls (empty circles and dashed line), nine evenly spaced carbonyls (filled triangles and solid line), 49 evenly spaced carbonyls (filled squares and solid line), and 9 evenly spaced groups of five carbonyls (empty triangles and dashed line). Inset is the same plot over a reduced pressure range to show detail. Lines are a guide for the eyes only. Refer to Fig. 1 for diagram of carbonyl configurations.

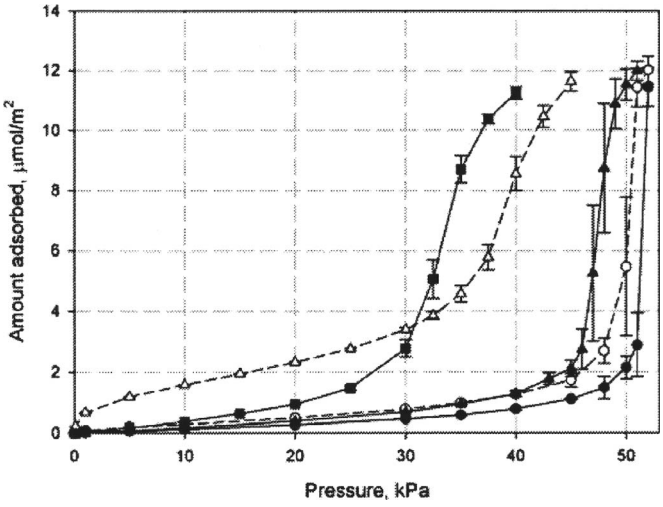

FIG. 3. Adsorption isotherms from simulation for ammonia at 240 K on graphite with various carbonyl configurations. Symbols as per Fig. 2.

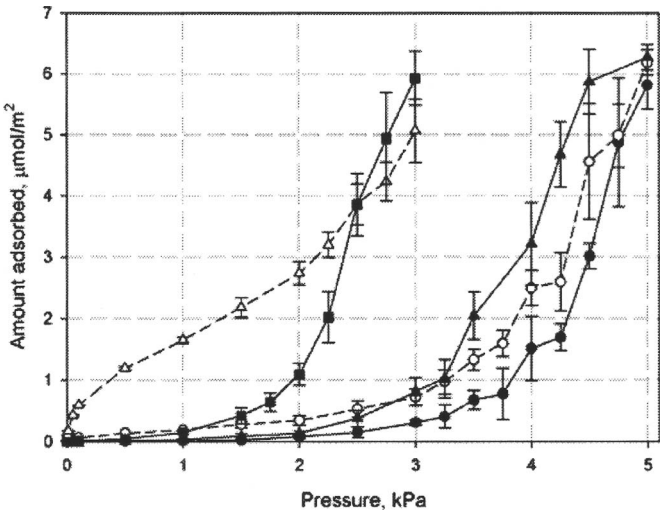

FIG. 4. Adsorption isotherms from simulation for methanol at 300 K on graphite with various carbonyl configurations. Symbols as per Fig. 2.

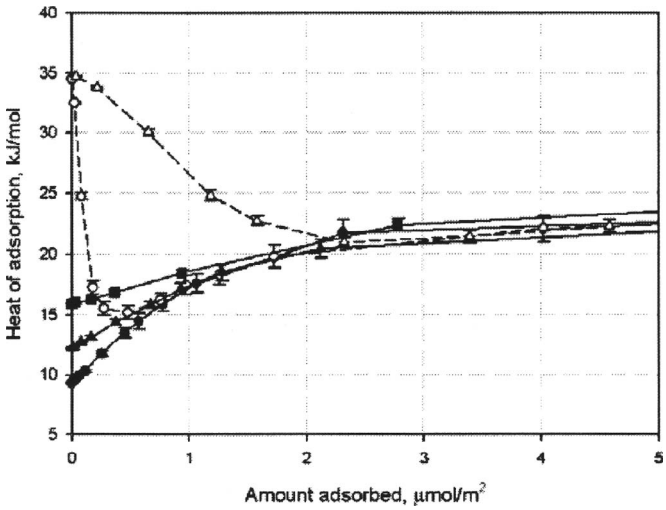

FIG. 6. Heat of adsorption from simulation for ammonia at 240 K on graphite with various carbonyl configurations. Symbols as per Fig. 2.

First the zero coverage heat of adsorption is increased due to the presence of the carbonyl groups. The zero coverage heats of adsorption are 9.45, 9.56, 9.57, 9.92, and 10.10 kJ/mol for the surface with no carbonyl groups, 5 grouped carbonyls, 9 evenly distributed carbonyls, 49 evenly distributed carbonyls, and nine groups of 5 carbonyls, respectively. So for the five grouped carbonyls and nine even carbonyls, the difference from the bare surface zero coverage heat of adsorption is small. For the nine groups of 5 carbonyls and 49 evenly spread carbonyls, the differences are much greater. The difference is sustained through monolayer coverage for the 49 evenly spread carbonyls but becomes very small for the nine groups of 5 carbonyls above 6 μmol/m^2. Over the range of 10–13 μmol/m^2, the heat of adsorption is much the same for all carbonyl configurations. However, a clear difference occurs between the heats of adsorption for the bare surface and the surface with the single group of five carbonyls and the rest of the carbonyl configurations. These two surfaces go through significant local maxima in their heats of adsorption at about 15.7 μmol/m^2 (at 16.6 kPa). Once the amount adsorbed reaches 20 μmol/m^2, the difference between these two surfaces and the rest has disappeared. This peak in the heat of adsorption is due to the freezing of the first layer and the associated change in energy of the system. This can be illustrated by looking at the density of the first layer of the system. From inspection of the density distribution[27] at 23.1 kPa, the first layer was defined as the midpoint between the peak in the first and second layer densities as indicated by the arrow in Fig. 8. Using this as the limit of the first layer, the surface density of the first layer can be calculated. The results of this calculation for the bare surface and the surface with 49 evenly spread functional groups are presented in Fig. 9 as a function of pressure.

Figure 9 shows that the density of the first layer for the bare surface appears to be reaching a maximum value up to a pressure of 12 kPa, and then increases markedly when the pressure reaches 16.6 kPa before reaching a maximum again at the higher pressures. In contrast the surface with 49 evenly distributed carbonyls has a smooth increase in the monolayer

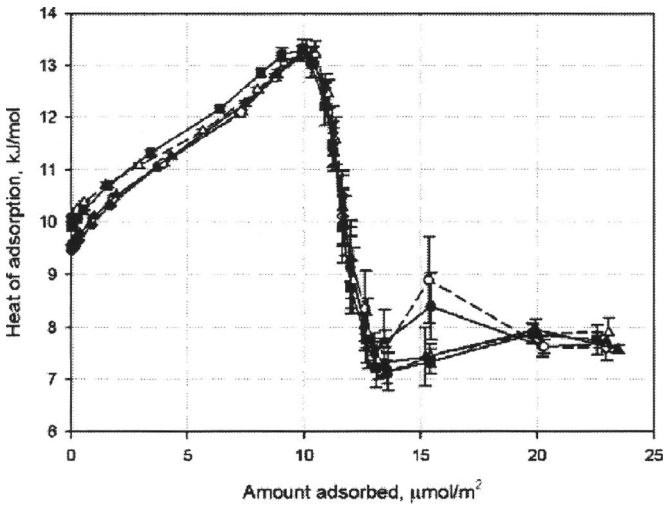

FIG. 5. Heat of adsorption from simulation for argon at 87.3 K on graphite with various carbonyl configurations. Symbols as per Fig. 2.

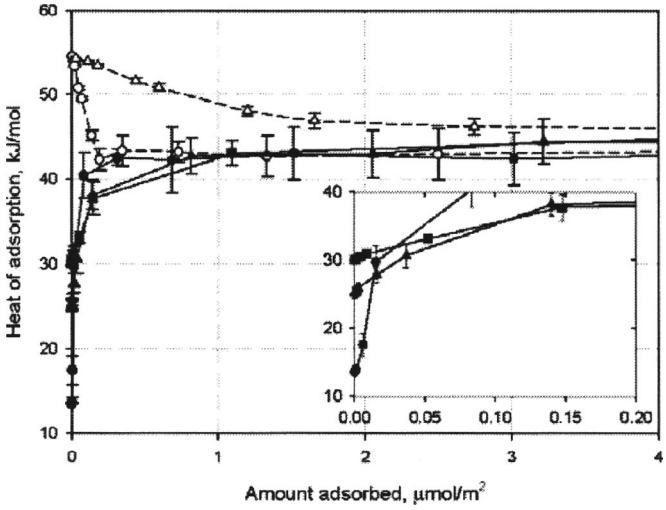

FIG. 7. Heat of adsorption from simulation for methanol at 300 K on graphite with various carbonyl configurations. Symbols as per Fig. 2.

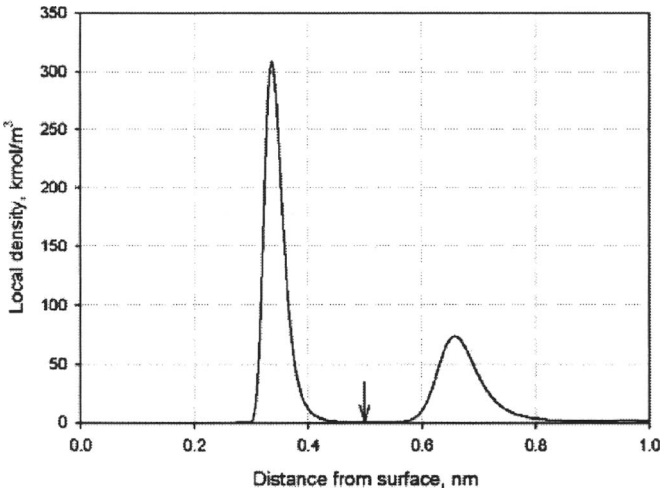

FIG. 8. Density distribution of argon at 87.3 K and 23.1 kPa on a bare surface versus distance from the surface.

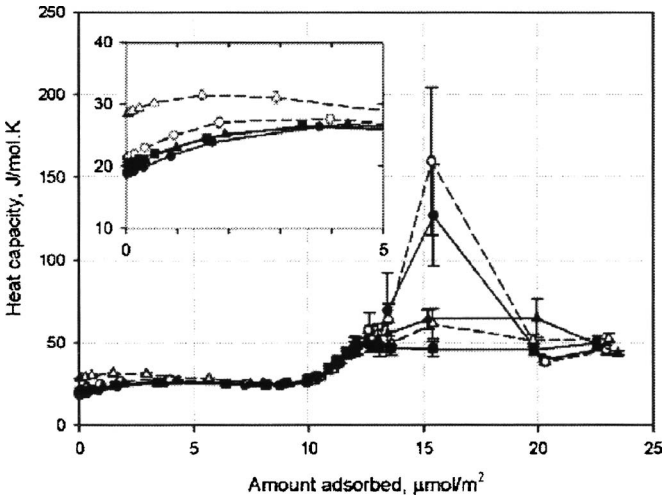

FIG. 10. Heat capacity from simulation for argon at 87.3 K on graphite with various carbonyl configurations. Inset shows the details of the plot at low coverage. Symbols as per Fig. 2.

density. So no transition to a solid first layer occurs if there is a large enough degree of heterogeneity on the surface.

The heats of adsorption for ammonia and methanol, in Figs. 6 and 7, respectively, are much more strongly affected by the carbonyl groups on the surface. As discussed by Birkett and Do,[2,14] the heat of adsorption is most strongly affected by the closely grouped carbonyls which act as an effective single high energy site. Once these sites are saturated, the adsorption of ammonia and methanol occurs by two dimensional clustering and the heat of adsorption approaches that of the bare surface.

Now that we have presented the isotherms and heats of adsorption, we can investigate the heat capacity of the adsorbed films. The heat capacities for the adsorbed films of argon at 87.3 K on various surfaces, using Eq. (3), are presented in Fig. 10. The contributions of the different components of the interaction energy to the heat capacity, calculated using Eq. (4), are presented in Fig. 11.

The heat capacity of argon in Fig. 10 shows some interesting features. The first and most dramatic is the very large peak in the heat capacity for the bare surface and the surface with a single group of five carbonyls. This occurs after the completion of the first layer at the same coverage as the local maximum in the isosteric heat as shown in Fig. 5. This is due to the transition to greater density in the first layer that was discussed earlier (Fig. 9). Figure 11 (plots *a* and *b*) shows that the peak in the heat capacity is a result of a peak in the both the fluid-fluid and fluid-solid contributions. The contribution of the fluid-functional contributions to the heat capacity is almost negligible in the case of a single group of five carbonyls. Upon heating, the first layer melts and expands to some degree pushing molecules from the first to the second layer. This can also be shown by repeating the calculations for Fig. 9 at a higher temperature. To this end, *nvt* simulations were performed for the bare surface at 91.3 K with the same loading as the GCMC simulation at 87.3 K. The density of the first layer versus total amount adsorbed at 87.3 and 91.3 K is plotted in Fig. 12.

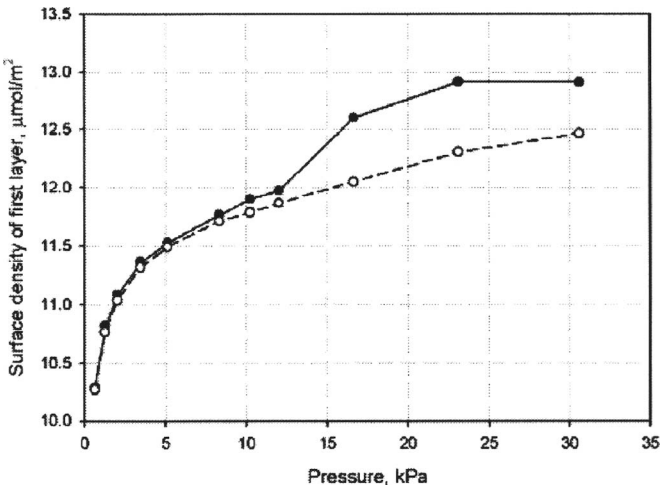

FIG. 9. Surface density of argon at 87.3 K in the first layer of adsorption versus pressure for a surface without carbonyls (filled circles and solid lines) and for a surface with 49 evenly distributed carbonyls (empty circles with dashed lines). Lines are a guide for the eyes only.

Figure 12 shows the change of density of the first layer with heating. Up to 10 μmol/m^2, where the transition to significant adsorption in the second layer occurs, the change in the density of the first layer when heated (from 87.3 to 91.3 K) is small. The difference upon heating becomes larger above 10 μmol/m^2 and undergoes a step change at a loading of 16.6 μmol/m^2 where the peak in the heat capacity occurs. This difference is sustained at higher loading even though the heat capacity comes down from its maximum. This may be due to the first layer melting at temperatures higher than 87.3 K, but less than 91.3 K, at these higher loadings. The movement of the molecules away from the surface to the second layer upon heating is associated with an expenditure of energy. Where the first layer transition is suppressed by evenly distributed single or grouped carbonyls, the peak in the heat capacity is greatly reduced [Figs. 11(c) and 11(d)]. For the 49 evenly spread carbonyls, which gives the most disrupted surface for argon packing, the peak in the heat capacity and its contribution from the fluid-fluid and fluid-solid interactions disappears completely. The contribution from fluid-functional interactions is low but

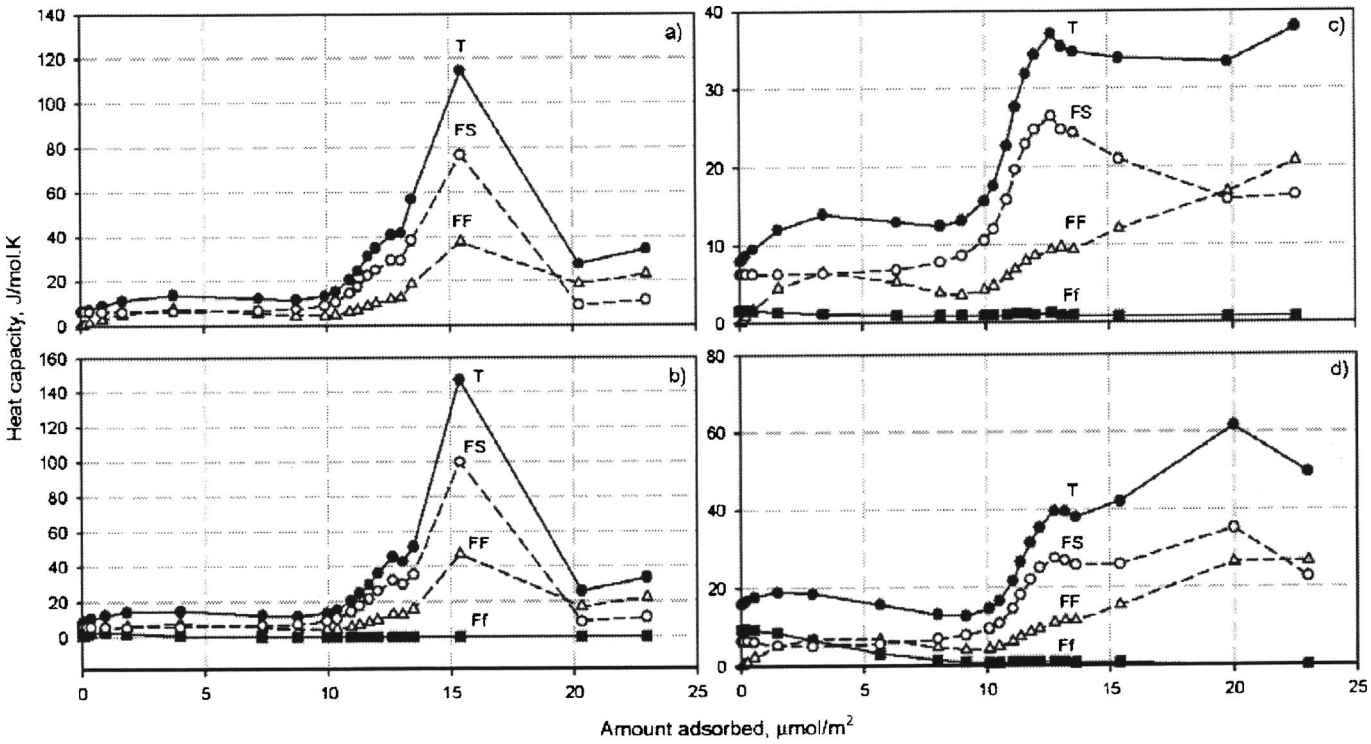

FIG. 11. Contributions to the heat capacity for argon at 87.3 K on graphite with (a) no functional groups, (b) 5 carbonyls, (c) 49 evenly distributed carbonyls, and (d) nine groups of 5 carbonyls. Total energetic contribution (T, filled circles), fluid-fluid contributions (FF, empty triangles), fluid-surface contributions (FS, empty circles), and fluid-functional contributions (Ff, filled squares). Lines are a guide for the eyes only. x axes of all plots have the same scale, but the scales of the *y* axes are as marked.

clearly greater than the case of a single group of five carbonyls. The surface with nine groups of five carbonyls has a small peak in the heat capacity at a higher loading (and pressure) than the bare surface. So the space between the groups of carbonyls must be sufficient for the packing, similar to that seen on the bare surface, to cause a peak in the solid-fluid contributions in Fig. 11(d).

The heat capacity for ammonia is presented in Fig. 13 for different carbonyl configurations, and its various contributions are presented in Fig. 14. Figure 13 shows a variety of behavior in the heat capacity curve depending on the carbonyl configuration. For the bare surface, the heat capacity rises to a maximum before decreasing again upon condensation to monolayer coverage. At monolayer coverage, approximately 11.5 μmol/m^2, all surfaces give the same heat capacity (within uncertainties of the simulation results) of 80 J/mol K. Figure 13 does not extend this far so that details at lower coverage can be more easily seen. However, the contributions to the heat capacity are plotted up to monolayer coverage in Fig. 14. In Fig. 14(a) we can see that the peak in the heat capacity for the bare surface is due exclusively to

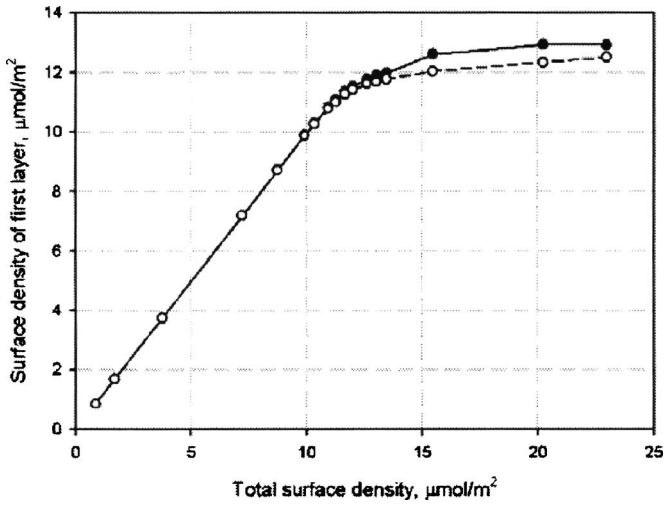

FIG. 12. Surface density of argon in the first layer of adsorption on a bare surface versus total surface density at 87.3 K (filled circles and solid lines) and 91.3 K (empty circles and dashed lines). Lines are a guide for the eyes only.

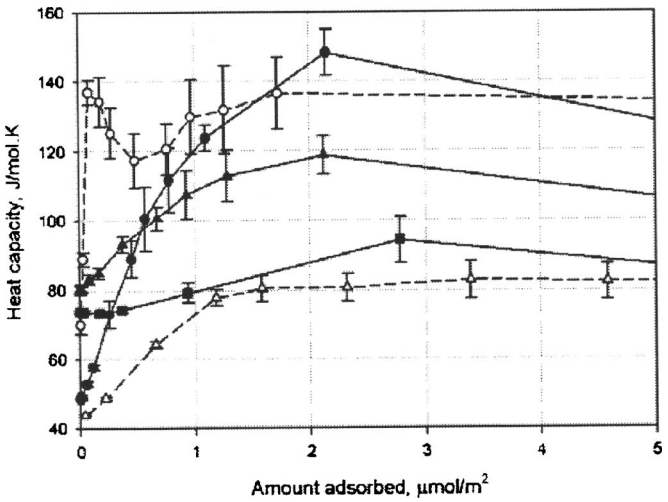

FIG. 13. Heat capacity from simulation for ammonia at 240 K on graphite with various carbonyl configurations. Symbols as per Fig. 2.

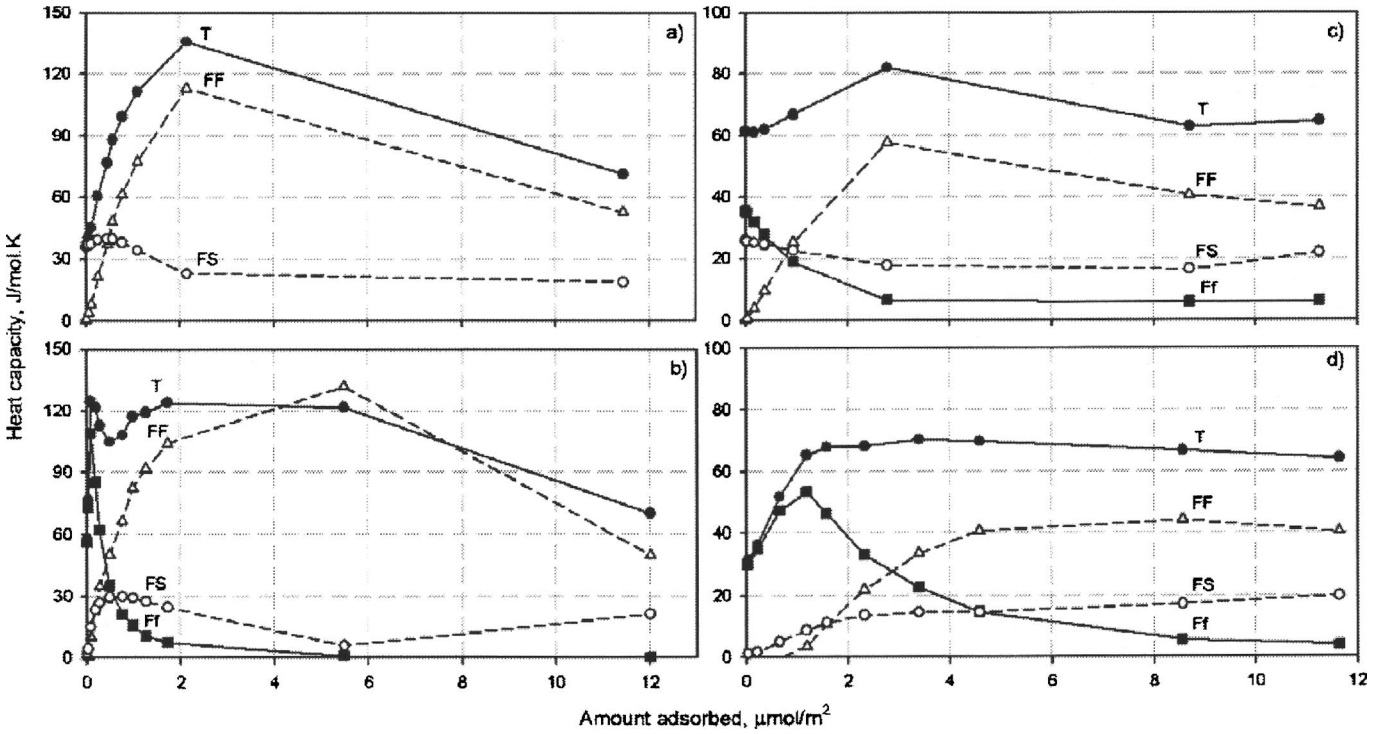

FIG. 14. Contributions to the heat capacity for ammonia at 240 K on graphite with (a) no functional groups, (b) 5 carbonyls, (c) 49 evenly distributed carbonyls, and (d) 9 groups of 5 carbonyls. Symbols as per Fig. 11.

the peak in the contribution from fluid-fluid interactions. The fluid-surface contributions are steady initially before decreasing as monolayer coverage is approached. In the course of calculations, fluid-fluid and fluid-functional contributions to the heat capacity were broken down to their LJ and Coulomb contributions. For both ammonia and methanol, the contributions are dominated by the Coulomb component. The LJ and Coulomb contributions are not plotted separately for clarity.

The fluid-fluid contributions are due to the breaking of bonds with near neighbors. Using radial distributions,[9] one can calculate the number of associated molecules per molecule in the simulation. For ammonia, we define an associated molecule as having a N–N separation of less than 0.51 nm. The number of associated molecules has been calculated for ammonia using *nvt* simulations, at the loadings presented in Fig. 3, at 240 and 244 K. The heat capacity versus the decrease in the number of associates, in heating from 240 to 244 K, is presented in Fig. 15(a). Using the same *nvt* simulations, it is possible to calculate the change in density in the first layer of ammonia by performing a similar analysis to that done for argon in Fig. 12. The first layer for ammonia is defined as up to 0.51 nm from the surface. The heat capacity versus the percentage change in the first layer density, in heating from 240 to 244 K, is given in Fig. 15(b).

So the heat capacity on the bare surface, at submonolayer coverage, is directly related to the decrease in the number of associated molecules upon heating. Only a small fraction of molecules leave the surface when heated, meaning disassociated molecules remain on the surface. Figure 15(b) shows that the change in density of the first layer upon heating is small (less than 2%) and not related to the increase in the heat capacity. This confirms, together with the fluid-solid contribution to the heat capacity in Fig. 14(a), that the desorption of ammonia from the first layer is not as important as the dissociation of clusters to the heat capacity.

For the case of nine evenly distributed carbonyls, the heat capacity curve is similar to that of the bare surface except that the peak in the heat capacity is shallower and the

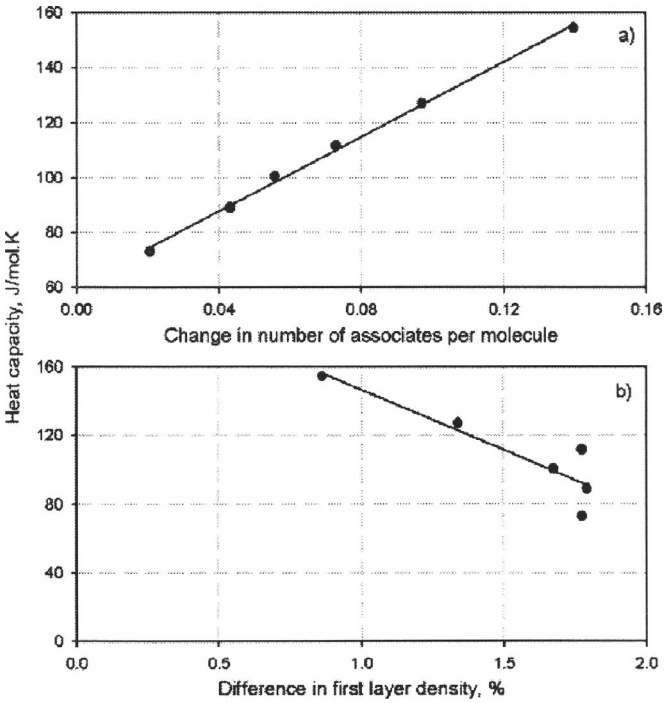

FIG. 15. Heat capacity vs the change in the number of associates per molecule (a) and the change in density of the first layer (b) for ammonia on a bare surface. The solid lines are linear regressions of plotted points.

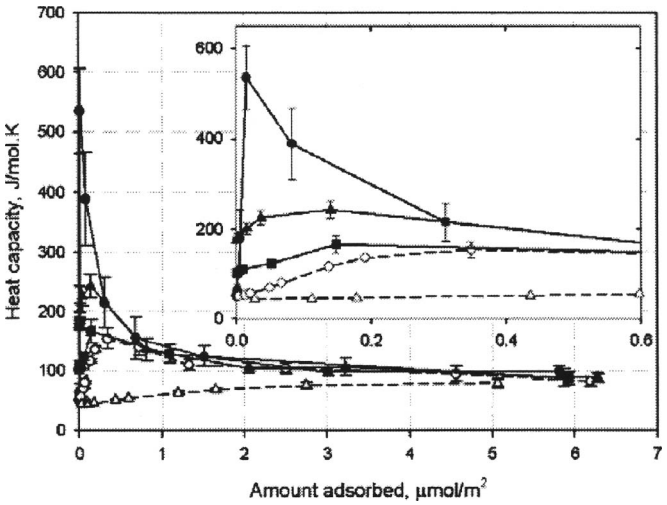

FIG. 16. Heat capacity from simulation for methanol at 300 K on graphite with various carbonyl configurations. Inset shows the details of the plot at low coverage. Symbols as per Fig. 2.

heat capacity at zero coverage is greater. In going from 9 evenly spread functional groups to 49, the peak becomes even shallower. The moderate peak is due to the fluid-fluid interactions and this contribution is much less than in the case of the bare surface [compare Figs. 14(a) and 14(c)]. The peak is also tempered by decreasing contributions from the fluid-surface and fluid-functional interactions. The heat capacity curve for the single group of five carbonyls (dashed line with open symbols in Fig. 13) is significantly different from the rest. It features a sharp local maximum at low coverage, followed by a local minimum before increasing again to approach the heat capacity on the bare surface. The sharp local maximum is due to the contributions from the fluid-functional interactions which peak at low coverage before falling away as coverage increases [Fig. 14(b)]. The fluid-fluid contributions to the heat capacity are similar to those of the bare surface, starting at zero and increasing with increasing coverage. The fluid-surface contributions differ between the two with the contribution starting at nearly zero and rising to a maximum before decreasing again for the surface with a single group of five carbonyls. When the number of groups of five carbonyls is increased to nine, similar behavior is seen but all peaks become smaller and shallower. Now we can identify several trends in the heat capacity with the addition of carbonyl groups. The addition of carbonyl groups reduces the fluid-solid contributions to the heat capacity, and the higher the attraction of the sites the greater the reduction. A greater number of carbonyl groups will reduce the zero coverage heat capacity and decrease and make shallower the peaks in any contribution to the heat capacity. We can now compare this to the behavior of another charged molecule, methanol.

The heat capacity for methanol is presented in Fig. 16 for different carbonyl configurations. The different contributions to the heat capacities of methanol are presented in Fig. 17. Let us first discuss the behavior of heat capacity for a bare surface. Figure 16 shows that the bare surface has a very large and sharp peak in the heat capacity. This sharp peak in the heat capacity is due solely to the fluid-fluid interactions. This is due to the hydrogen bonding between the methanol molecules and was shown by Birkett and Do[2] to be directly related to the degree of clustering of the methanol. However, the degree of clustering is not really the property that defines the heat capacity but the change in clustering upon heating.

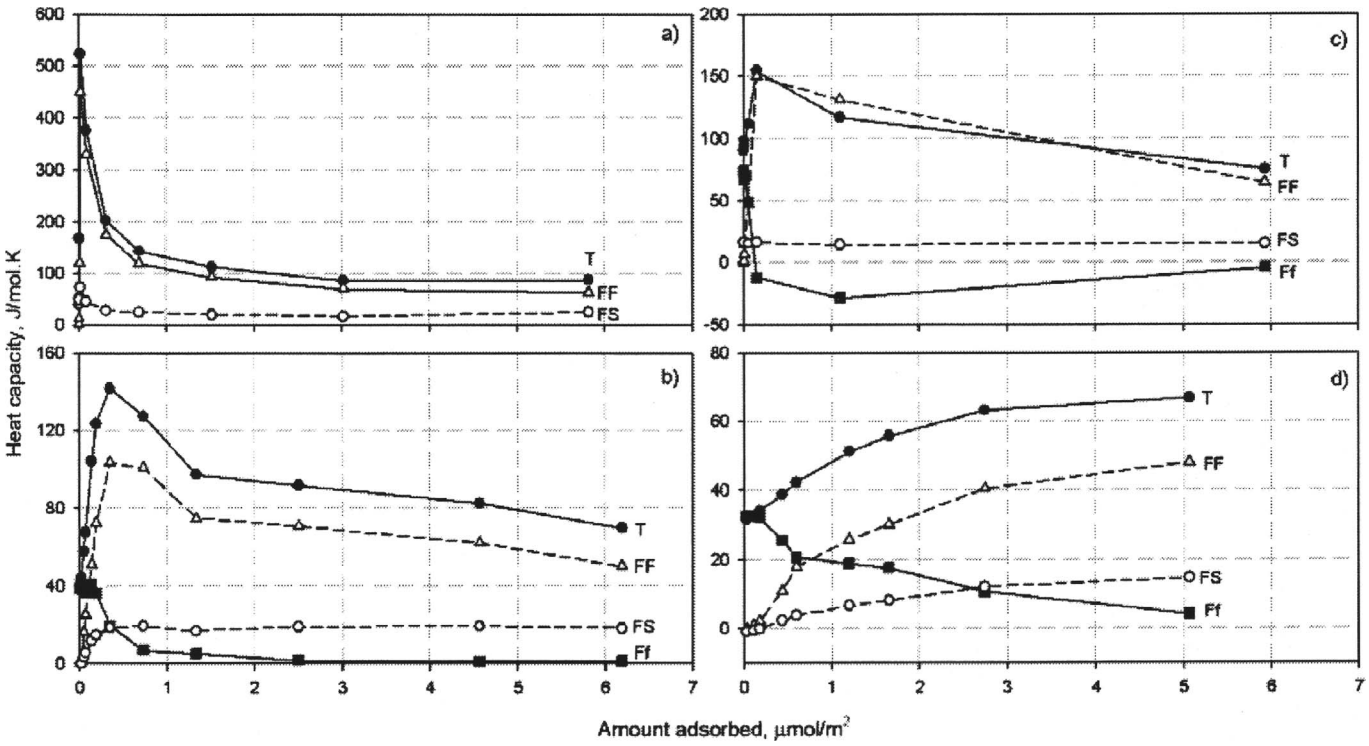

FIG. 17. Contributions to the heat capacity for methanol at 300 K on graphite with (a) no functional groups, (b) 5 carbonyls, (c) 49 evenly distributed carbonyls, and (d) nine groups of 5 carbonyls. Symbols as per Fig. 11.

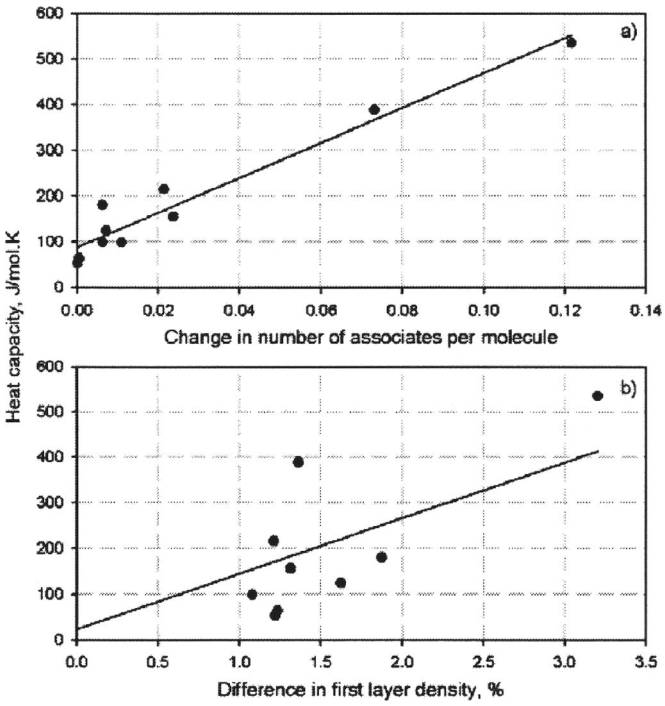

FIG. 18. Heat capacity vs the change in the number of associates per molecule (a) and the change in density of the first layer (b) for methanol on a bare surface. The solid lines are linear regressions of plotted points.

This can be investigated in the same manner as was done with ammonia above. The number of associated molecules for each methanol has been calculated at 300 and 304 K for the same loadings on the bare surface as shown in Fig. 4. Two methanol molecules are defined as being associated when their O–H separation is less than 0.26 nm. The heat capacity versus the decrease in the number of associated methanol molecules upon heating, from 240 to 244 K, is plotted in Fig. 18(a). The heat capacity versus the percentage decrease in the density of the first layer is presented in Fig. 18(b).

Figure 18(a) shows that the methanol heat capacity is directly related to the reduction in the hydrogen bonding of the methanol molecules in submonolayer coverage. There is a small decrease in the density of the first layer upon heating (less than 3%). This change in the first layer density has some correlation with the heat capacity, but its contribution to the heat capacity is small compared with the breaking of fluid-fluid hydrogen bonds [comparing contributions in Fig. 17(a)]. The small change in the first layer density indicates that the decreased hydrogen bonding results in mostly a more dispersed methanol phase on the surface rather than methanol leaving the surface. The correlation between heat capacity and dissociation and the tendency of disassociated molecules to stay the surface are similar to the trends seen for ammonia (Fig. 15). However, for methanol the peak is much sharper in the heat capacity and occurs at much lower loading. This is a result of the methanol associating in smaller dispersed clusters. So the location and intensity of heat capacity peaks could be used for the determination of the nature of surface clustering.

Now when the surface has a single group of five carbonyls [Figs. 16 and 17(b)], the peak in the heat capacity is reduced due to a corresponding decrease in the peak of the fluid-fluid contributions. The fluid-surface contributions are reduced initially and rise from zero before reaching the same stable value as the bare surface at higher coverages. The fluid-functional contributions are significant at low coverage before decreasing to zero as the adsorption increases. Increasing the number of groups of five carbonyls to nine results in a similar trend to that seen for ammonia. Figure 17(d) shows the spread of the heat capacity contributions due to the larger number of groups. The fluid-surface and fluid-functional contributions, while changing over a wider range of coverage, maintain similar values to those for the single group of five carbonyls. However, the fluid-fluid contributions are significantly reduced for the case of the surface with nine groups. For the case of 9 and 49 evenly distributed carbonyls, the peak is sharper and higher than for the surface with grouped carbonyls. Figure 17(c) shows that for the case of 49 evenly distributed carbonyls, the peak is still due to the fluid-fluid interactions. The fluid-functional contributions are much greater than for the case of grouped carbonyls initially but quickly decay to make a negative contribution to the heat capacity at higher coverages. The fluid-surface contributions are relatively constant through the range of adsorption studied and are greater than in the case of grouped carbonyls but less than the bare surface. So like ammonia, the addition of carbonyl groups reduces the fluid-solid and fluid-fluid contributions to the heat capacity, with the reduction being the greatest in the case of grouped carbonyls. A greater number of evenly spaced carbonyls reduces the zero coverage heat capacity, but the number of groups of carbonyls does not seem to affect this.

V. CONCLUSIONS

Adsorption isotherms, heats of adsorption, and heat capacities of the adsorbed phases have been calculated for argon at 87.3 K, ammonia at 240 K, and methanol at 300 K. The adsorption of each of these fluids has been simulated on a bare graphite surface and surfaces with different configurations of functional groups. The carbonyl groups had a small impact on the adsorption isotherms of argon in the transitions to monolayer coverage and had a major effect on the isotherms of ammonia and methanol up to monolayer coverage. Isosteric heats of argon are affected, in general, a small amount, by the presence of the functional groups. However, for the bare surface there exists a significant peak in the heat of adsorption shortly after monolayer coverage. This peak is a due to a phase transition in the first layer and disappears if the surface has many dispersed carbonyl groups. The heat capacities of ammonia and methanol are strongly affected, in qualitatively similar ways, by the presence of functional groups.

In addition to heat capacities, the individual energetic contributions to the heat capacity have been calculated. The transition of the first layer in argon adsorption results in a dramatic peak in the heat capacity, which is much more pronounced than the corresponding peak in the heat of adsorption. The peak is the result of fluid-surface and fluid-fluid interactions. Sufficiently dispersed functional groups reduce

this peak. Ammonia and methanol, qualitatively similar in terms of heats of adsorption, give qualitatively different heat capacity behaviors. Methanol has its greatest heat capacity at low coverage on a bare surface due to fluid-fluid interactions. Addition of any functional groups reduces and spreads this peak. Ammonia does not have the same extreme peak in its heat capacity on the bare surface and shows particularly different behavior for the case of five closely grouped carbonyls. The contrast in the bare surface heat capacities between methanol and ammonia provides a clear indicator of the different clusterings of the two fluids on the surface.

ACKNOWLEDGMENTS

This research was made possible by the Australian Research Council whose support is gratefully acknowledged. Thanks also to the University of Queensland High Performance Computing facility for a generous allocation of computing time.

[1] D. Frenkel and B. Smit, *Understanding Molecular Simulation*, 2nd ed. (Academic, San Diego, 2002).
[2] G. R. Birkett and D. D. Do, Mol. Simul. **32**, 887 (2006).
[3] B. Chen, J. J. Potoff, and J. I. Siepmann, J. Phys. Chem. B **105**, 3093 (2001).
[4] T. Kristof, J. Vorholz, J. Liszi, B. Rumpf, and G. Maurer, Mol. Phys. **97**, 1129 (1999).
[5] A. Michels, H. Wijker, and H. Wijker, Physica (The Hague) **15**, 627 (1949).
[6] A. Z. Panagiotopoulos, Mol. Phys. **61**, 813 (1987).
[7] A. Z. Panagiotopoulos, N. Quirke, M. Stapleton, and D. J. Tildesley, Mol. Phys. **63**, 527 (1988).
[8] W. A. Steele, Surf. Sci. **36**, 317 (1973).
[9] M. P. Allen and T. P. Tildesley, *Computer Simulation of Liquids* (Clarendon, Oxford, 1987).
[10] M. Jorge and N. A. Seaton, Mol. Phys. **100**, 3803 (2002).
[11] W. L. Jorgensen and J. Tirado-Rives, J. Am. Chem. Soc. **110**, 1657 (1988).
[12] M. Jorge, C. Schumacher, and N. A. Seaton, Langmuir **18**, 9296 (2002).
[13] G. R. Birkett and D. D. Do, Mol. Phys. **104**, 623 (2006).
[14] G. R. Birkett and D. D. Do, Mol. Simul. **32**, 523 (2006).
[15] T. Morimoto and K. Miura, Langmuir **1**, 658 (1985).
[16] T. Morimoto and K. Miura, Langmuir **2**, 43 (1986).
[17] B. Chen and J. I. Siepmann, J. Phys. Chem. B **105**, 11275 (2001).
[18] D. M. Heyes and F. Van Swol, J. Chem. Phys. **75**, 5051 (1981).
[19] M. Jorge and N. A. Seaton, Mol. Phys. **100**, 2017 (2002).
[20] D. M. Heyes, M. Barber, and J. H. R. Clarke, J. Chem. Soc., Faraday Trans. 2 **73**, 1485 (1977).
[21] A. V. Shevade, S. Y. Jiang, and K. E. Gubbins, Mol. Phys. **97**, 1139 (1999).
[22] A. Striolo, A. A. Chialvo, P. T. Cummings, and K. E. Gubbins, Langmuir **19**, 8583 (2003).
[23] A. Striolo, K. E. Gubbins, A. A. Chialvo, and P. T. Cummings, Mol. Phys. **102**, 243 (2004).
[24] A. Striolo, K. E. Gubbins, M. S. Gruszkiewicz, D. R. Cole, J. M. Simonson, and A. A. Chialvo, Langmuir **21**, 9457 (2005).
[25] A. Striolo, A. A. Chialvo, K. E. Gubbins, and P. T. Cummings, J. Chem. Phys. **122**, 234712/1 (2005).
[26] J. C. Liu and P. A. Monson, Langmuir **21**, 10219 (2005).
[27] D. Nicholson and N. G. Parsonage, *Computer Simulation and the Statistical Mechanics of Adsorption* (Academic, London, 1982).
[28] P. Schofield, Proc. Phys. Soc. London **88**, 149 (1966).
[29] N. N. Avgul and A. V. Kiselev, Chem. Phys. Carbon **6**, 1 (1970).